

Bayesian LSTM for indoor temperature modeling

Emma Hannula^{a,c,*}, Arttu Häkkinen^{a,b,*}, Antti Solonen^{a,b}, Felipe Uribe^{a,b}, Jana de Wiljes^{a,c}, Lassi Roininen^a

^a*LUT University, Yliopistonkatu 34, Lappeenranta, 53850, Finland*

^b*Danfoss Leanheat, Ilmalantori 1, Helsinki, 00240, Finland*

^c*TU Ilmenau, Ehrenbergstraße 29, Ilmenau, 98693, Germany*

Abstract

Improving energy efficiency of building heating systems is essential for reducing global energy consumption and greenhouse gas emissions. Traditional control methods in buildings rely on static heating curves based solely on outdoor temperature measurements, neglecting system state and free heat sources like solar gain. Model predictive control (MPC) not only addresses these limitations but further optimizes heating control by incorporating weather forecasts and system state predictions. However, current industrial MPC solutions often use simplified physics-inspired models, which compromise accuracy for interpretability. While purely data-driven models offer better predictive performance, they face challenges like overfitting and lack of transparency.

To bridge this gap, we propose a Bayesian Long Short-Term Memory (LSTM) architecture for indoor temperature modeling. Our experiments across 100 real-world buildings demonstrate that the Bayesian LSTM outperforms an industrial physics-based model in predictive accuracy, enabling potential for improved energy efficiency and thermal comfort if deployed in heating MPC solutions. Over deterministic black-box approaches, the Bayesian framework provides additional advantages by improving generalization ability and allowing interpretation of predictions via uncertainty quantification. This work advances data-driven heating control by balancing predictive performance with the transparency and reliability required for real-world heating MPC applications.

Keywords: Model predictive control, Bayesian neural networks, Long short-term memory, Uncertainty quantification, Central heating systems

1. Introduction and scope

Heating of buildings contributes significantly to global energy use and greenhouse gas emissions [1, 2, 3, 4], especially in northern climates with long and cold winters [5]. Global warming and Europe's recent energy crisis further highlight the need for energy-efficient heating solutions.

Water-based central heating systems, often using district heating as the heat source, dominate northern climates, particularly in urban multi-apartment buildings. These systems consist of two networks separated by heat exchangers: the primary side (connected to the heat source) and the secondary side (distributing heat within the building). The secondary side typically includes circuits for domestic hot water and space heating. A heat controller adjusts primary-side flow via control valves to regulate secondary-side temperatures. In this study, we focus on Nordic residential buildings with radiator or underfloor heating systems.

Traditional control relies on a deterministic heating curve, reactively adjusting space heating supply temperature based on measured outdoor temperature. However, this open-loop approach lacks feedback on the state of the system (indoor temperature), often leading to inefficiencies via over- or underheating. It also lacks in ability to anticipate sudden weather changes and account for factors bringing free heat to the system, like solar irradiation and internal heat sources (e.g., occupants and electronic devices). The thermal dynamics of buildings evolve constantly, and therefore determining a suitable heating curve is often done via endless loop of trial and error, otherwise requiring expensive expert services or complex physics-based white-box modeling.

*Corresponding authors.

Email addresses: emma.hannula@lut.fi (Emma Hannula), arttu.hakkinen@lut.fi (Arttu Häkkinen)

These shortcomings can be addressed with model predictive control (MPC), which closes the feedback loop by exploiting system state measurements, and additionally utilizes weather forecasts to plan control actions into the future [6, 7]. Predictive indoor temperature models – formulated to capture building thermal dynamics – are central to MPC, allowing the inclusion of such factors as solar irradiation and temporal disturbances from internal heat sources to the equation. These models adapt to the current heating dynamics of the buildings constantly via automatic updates based on new data. Hence, MPC provides actual control of the system state, often resulting in reduced energy use.

MPC enables the incorporation of additional optimization objectives such as peak load minimization by shifting heating loads based on predictive modeling and temporal profiles of domestic hot water usage learned from data. Moreover, district heating utilities can use MPC-controlled building stocks as thermal storages when optimizing their production planning, since the heat loads inside the buildings can be controlled more accurately. To achieve all this, accurate indoor temperature predictions are crucial, especially into longer prediction horizons.

MPC applications can be classified according to the indoor temperature modeling approach: white-, grey-, and black-box [8]. White-box models are fully physics-based, relying on theoretical principles of heat transfer and energy conservation, and building metadata. While being interpretable, they are often impractical for scalable solutions. Grey-box models combine physics-inspired equations with statistical parameter estimation. They are robust and interpretable, but often oversimplify complex dynamics such as thermal lag effects. Black-box models are purely data-driven alternatives, capable of capturing even the complex nonlinear relationships in the presence of large and descriptive datasets about the system inputs and state evolution. However, they risk overfitting and lack interpretability; therefore, asking for some form of uncertainty quantification to be viable for real-world applications.

Related work. Research in machine learning for time series modeling has predominantly concentrated on exploring recurrent neural networks (RNNs) for specific applications. For example, Ramadan et al. [9] applied multiple machine learning methods for indoor temperature prediction and compared their performance against a resistance-capacity grey-box model. Among these techniques, the long short-term memory (LSTM), a type of RNN, has been proven to provide even more accurate results [10, 11, 12]. Consequently, recent studies have aimed to enhance LSTM accuracy by employing methods such as feature extraction with convolutional layers [13], and incorporating an encoder-decoder architecture with Bayesian hyperparameter optimization [14]. Fang et al. [15] highlighted the effectiveness of LSTM models when trained on extensive datasets, such as three years of data. However, despite showing promising results, many of these methods are primarily validated through simulations and lack application to real-world buildings [16].

Existing applications of uncertainty quantification for machine learning in the context of time series models include the following. The Bayesian RNN model discussed in [17], which employs a sequential approach to update network parameters and hyperparameters, outperforms several traditional time series modeling methods. Another development is the quantile RNN model proposed in [18], which directly learns prediction intervals as lower and upper bounds; this model effectively handles multiple time series, shifting seasonality, future planned event spikes, and cold-starts in large-scale forecasting scenarios. Frequentist approaches to uncertainty estimation are also available. For instance, the method in [19] derives predictive uncertainty from the variability of the RNN output’s sampling distribution; this is achieved by repeatedly removing sections of temporally correlated training data and collecting predictions from the RNN re-trained on the remaining data. Conformal prediction has gained popularity as a frequentist method for constructing distribution-free prediction intervals. However, since this approach requires data exchangeability, which is often not applicable in time series, the methods in [20, 21] propose techniques to extend its applicability to time series data.

Contributions and novelty. The main contributions of the paper are highlighted as follows:

- (i) We derive a Bayesian grey-box model for indoor temperature that has been successfully integrated into an industrial MPC solution currently operating across nearly 4,000 central-heated buildings.
- (ii) We develop and implement a Bayesian LSTM approach for indoor temperature modeling that provides prediction uncertainty quantification, offering enhanced interpretability over deterministic LSTM methods with negligible sacrifices in predictive performance.
- (iii) Our results demonstrate that the Bayesian LSTM achieves significantly better predictive performance than the reference model across 100 real-world buildings. Implementing this model in MPC would improve control of central-heated buildings by enhancing both energy efficiency and indoor comfort.

Structure of the paper. This paper is organized as follows. In Section 2, we introduce the reference model and the proposed Bayesian LSTM. Section 3 outlines the used dataset, experiments, and results. Section 4 presents the concluding remarks of the study.

2. Methodology

We introduce the reference grey-box model and the deep learning models for predicting the indoor temperature of central-heated residential buildings. The reference model and the Bayesian deep learning model have built-in uncertainty quantification via their parameter estimation approach, and hence, we start by covering the theoretical principles behind the Bayesian framework.

2.1. Bayesian inference

In the Bayesian framework, model unknowns are represented through probability distributions, which inherently incorporate the existing uncertainty [22]. Particularly, Bayesian inference allows updating beliefs about unknown quantities \mathbf{Z} of a mathematical model given observed data $\mathbf{y} \sim \mathbf{Y}$. At its core, Bayesian inference is based on Bayes' theorem, for which the main components are the *prior*, the *likelihood*, and the *posterior*.

- The prior distribution $p(\mathbf{Z})$, expresses the initial beliefs, assumptions, or knowledge about \mathbf{Z} without observing any data.
- The likelihood function $p(\mathbf{y} | \mathbf{Z})$, quantifies the probability of observing the data \mathbf{y} given a specific realization of $\mathbf{Z} = \mathbf{z}$, thus reflecting how well the observations support our computational model.
- The posterior distribution $p(\mathbf{Z} | \mathbf{y})$ represents the updated beliefs about \mathbf{Z} after observing \mathbf{y} . It combines the prior assumptions with the new information provided by the data through Bayes' theorem:

$$p(\mathbf{Z} | \mathbf{y}) = \frac{p(\mathbf{y} | \mathbf{Z})p(\mathbf{Z})}{p(\mathbf{y})}, \quad (1)$$

where $p(\mathbf{y}) = \int p(\mathbf{y} | \mathbf{Z}) d\mathbf{p}(\mathbf{Z})$ is the marginal likelihood or evidence, which acts as a normalizing constant.

The primary objective of Bayesian inference is then to find the posterior probability density $p(\mathbf{Z} | \mathbf{y})$. In practice, this task is often computationally intractable, primarily due to the high dimensionality of \mathbf{Z} and the complexity of the computational model. As a result, we are forced to settle for approximations.

Variational inference. The posterior can be approximated either using sampling-based methods such as Markov Chain Monte Carlo (MCMC) [22] or the framework of *variational inference* [23, 24, 25, 26]. Although the former is often capable of achieving more precise approximations, the latter is far more computationally efficient. Hence, for the posterior inference of the models covered in this study for large-scale industrial solutions, we focus on variational inference.

In variational inference, the aim is to find the reference parameters of a tractable variational distribution $q(\mathbf{Z})$ such that it approximates the true posterior $p(\mathbf{Z} | \mathbf{y})$ as closely as possible [25]. This closeness is measured using the Kullback–Leibler (KL) divergence, which by definition, measures the dissimilarity between two distributions, for instance:

$$D_{KL}(q(\mathbf{Z}) \| p(\mathbf{Z} | \mathbf{y})) = \int q(\mathbf{Z}) \log \left(\frac{q(\mathbf{Z})}{p(\mathbf{Z} | \mathbf{y})} \right) d\mathbf{Z} \geq 0. \quad (2)$$

Consequently, the problem of posterior inference is transformed into an optimization problem of minimizing the KL divergence in (2), which is equivalent to maximizing an alternative quantity, the evidence lower bound (ELBO) [23, 24],

$$\text{ELBO}(q) = \mathbb{E}_q[\log p(\mathbf{y} | \mathbf{Z})] - D_{KL}(q(\mathbf{Z}) \| p(\mathbf{Z})), \quad (3)$$

to achieve the tightest bound on the logarithmic marginal likelihood $\log p(\mathbf{y})$.

Maximizing (3) with respect to $q(\mathbf{Z})$ can be done using multiple methods, but typically they ensure tractability by assuming the unknowns as independent, factorizing according to mean-field approximation [24] as

$$q(\mathbf{Z}) = \prod_i q(\mathbf{Z}_i). \quad (4)$$

While there are some specific forms of variational families for which the optimization problem can be solved in closed form, in practice, this is typically feasible only for distributions from the conjugate exponential family.

2.2. Reference model

Under steady-state conditions, let us consider the air mass inside a building as a system, separated from its surroundings by the building envelope (cf. Figure 1). The envelope and surroundings are treated as homogeneous media with uniform thermal properties. While buildings typically have multiple thermal zones, we simplify the inner volume as a single room. Additionally, we assume that the envelope has minimal thermal capacitance, acting only as a thermal resistor for heat flow between the system and the environment.

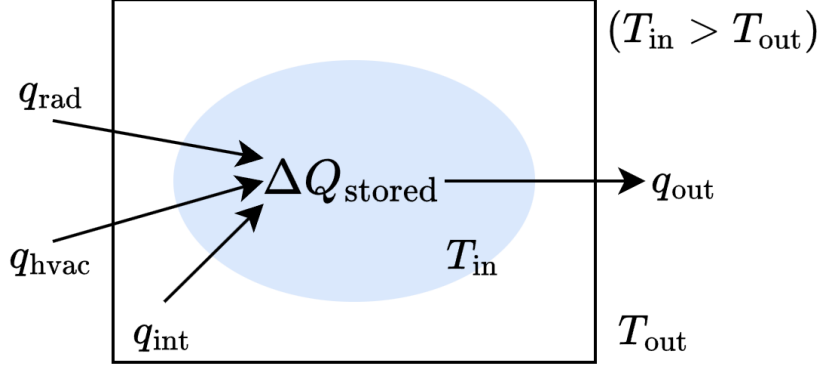


Figure 1: Conservation of thermal energy in a building. Here $\Delta Q_{\text{stored}} = \frac{dQ_{\text{stored}}}{dt}$ describes the rate of change of the thermal energy stored by the indoor air mass over time t .

This first-order nodal view of a highly complex and time-varying dynamical system [27] provides a generalizable basis for scalable MPC solutions without the need for human interference in model calibration. Although higher-order models would perform well in ideal scenarios, our practical experience indicates that implementing second-order approaches, which consider the envelope's thermal capacitance, presents significant challenges at an industrial scale. These challenges arise primarily due to the introduction of additional latent states and the difficulties in achieving robust parameter estimation from noisy data.

According to the basic physics principle of energy conservation, the change in the thermal energy stored by a system must be equal to the sum of heat flows entering and leaving the system. Applying this and adopting the notation in Figure 1, the thermal energy balance equation for a building can be written as

$$\frac{dQ_{\text{stored}}}{dt} = q_{\text{hvac}} + q_{\text{out}} + q_{\text{rad}} + q_{\text{int}}, \quad (5)$$

where $\frac{dQ_{\text{stored}}}{dt}$ is the rate of change of thermal energy stored by the indoor air mass with respect to time, q_{hvac} is the heat flow from the heating, ventilation and air conditioning (HVAC) system, q_{out} is the heat flow through the building envelope, q_{rad} is the heat flow from solar irradiation, and q_{int} is the combined heat flow from a variety of building's internal heat sources. Here, all right-hand side terms are nonnegative except for q_{out} , assuming that the indoor temperature is greater than the outdoor temperature.

Let us consider that q_{hvac} is brought to the system by a single radiator, which is also a straight pipe, thus assuming the heat flows from other heat sources as negligible. Furthermore, we treat the conductive thermal resistance of the envelope and the convective thermal resistances at its boundary air layers as a single lumped thermal resistor. Expanding the terms in (5) according to heat transfer equations, rearranging, and denoting the unknown physical coefficients as the parameter vector $\theta \in \mathbb{R}^d$, yields a first-order ordinary differential equation (ODE) for indoor temperature:

$$\frac{dT_{\text{in}}}{dt} = \theta_1(T_{\text{sup}} - T_{\text{in}}) + \theta_2(T_{\text{out}} - T_{\text{in}}) + \theta_3\Phi_{\text{rad}} + \psi(t), \quad (6)$$

where T_{sup} is the space heating supply water temperature, T_{in} is the indoor temperature, T_{out} is the outdoor temperature, and Φ_{rad} is the global horizontal irradiation intensity of the sun. For the q_{int} term in (5), even a simplified physical formula cannot be devised. However, it can be assumed that the effect of this term has some kind of temporal profile, which can be learned from the data. In this work, the hours of the week are divided into 24 business-day and 24 non-business-day hours (weekends and public holidays), summing up to 48 hourly disturbance profiles for internal sources. Thus, q_{int} is written as an

indicator function ψ mapping time t to 48 parameters based on the hour of the week. The variables in the other terms are obtained as measured inputs.

Linear state-space models (LSSM) are widely used in control theory, time series analysis, and modeling of dynamical systems [28, 29, 26]. Thus, it is convenient to formulate (6) as an LSSM by including process and observation noise terms, which are assumed to be Gaussian with zero mean and unknown covariances. This yields the following probabilistic representation for state transition

$$\begin{aligned} \hat{x}^{(t)} &= (1 - \theta_1 - \theta_2)\hat{x}^{(t-1)} + \begin{bmatrix} \theta_1 & \theta_2 & \theta_3 & 1 \end{bmatrix} \begin{bmatrix} T_{\text{sup}}^{(t)} \\ T_{\text{out}}^{(t)} \\ \Phi_{\text{rad}}^{(t)} \\ \psi(t) \end{bmatrix} + \mathcal{N}(0, \theta_4^{-1}) \\ y^{(t)} &= \hat{x}^{(t)} + \mathcal{N}(0, \theta_5^{-1}), \end{aligned} \quad (7)$$

where $\hat{x}^{(t)}$ is the estimated indoor temperature state at time t , and $y^{(t)}$ is the measured indoor temperature at time t . For this, the continuous time is discretized based on the resolution of the available measurement data, and the LSSM in (7) is solved via Kalman filtering [26, 30]. In this work, the time resolution is hourly. Collectively, the model parameters, noise parameters, and hourly profile parameters result in the LSSM described in (7) having a total of $D = 53$ parameters. Moreover, let us denote N as the number of total observations, such that $\mathbf{y} = [y^{(1)}, \dots, y^{(N)}]$.

The state and parameter estimation for the LSSM model (7) is implemented through the Bayesian framework introduced in 2.1. The joint posterior can be written as

$$p(\hat{\mathbf{x}}, \boldsymbol{\theta}, \boldsymbol{\alpha} \mid \mathbf{y}) \propto p(\mathbf{y} \mid \hat{\mathbf{x}}, \boldsymbol{\theta}) p(\hat{\mathbf{x}} \mid \boldsymbol{\theta}) p(\boldsymbol{\theta} \mid \boldsymbol{\alpha}) p(\boldsymbol{\alpha}), \quad (8)$$

where $p(\mathbf{y} \mid \hat{\mathbf{x}}, \boldsymbol{\theta})$ is the likelihood function after observing the data \mathbf{y} and $p(\hat{\mathbf{x}} \mid \boldsymbol{\theta})$ is the state prior probability. Both of these are Gaussian densities derived based on (7). Furthermore, we assign conjugate-exponential priors to the remaining terms in (8) such that

$$p(\boldsymbol{\theta} \mid \boldsymbol{\alpha}) = \prod_{i=1}^D \mathcal{N}(\theta_i \mid 0, \alpha_i^{-1}) \quad p(\boldsymbol{\alpha}) = \prod_{i=1}^D \mathcal{G}(\alpha_i \mid a, b), \quad (9)$$

where the hyperparameters a and b are defined with non-informative priors.

Since the model is used in a large-scale industrial application, employing sampling-based methods such as MCMC for posterior inference is impractical. This is primarily due to the complex geometry of the posterior and the fact that evaluating the posterior for a single sample requires a complete solution of the Kalman filter [26, 30]. Consequently, we seek an approximate solution of the posterior in (8) using variational inference as described in 2.1, by assuming the following factorization with respect to the model unknowns:

$$p(\mathbf{Z} \mid \mathbf{y}) \approx q(\mathbf{Z}) = q(\hat{\mathbf{x}})q(\boldsymbol{\theta})q(\boldsymbol{\alpha}), \quad (10)$$

where we denote $\mathbf{Z} = \{\hat{\mathbf{x}}, \boldsymbol{\theta}, \boldsymbol{\alpha}\}$ as a set of all unknowns in (8). Each component of the factorized variational approximation in (10) has the same family as the prior on the respective unknown variable, with its own reference parameters. To find these parameters, the ELBO in (3) is maximized using the posterior (8) and its approximation (10) via the Variational Message Passing (VMP) algorithm [25]. Given our conjugate-exponential assumptions, VMP offers a computationally efficient solution for the posterior approximation, while still offering a full probabilistic framework for state and parameter estimation, unlike methods such as the maximum a posteriori estimator. Both the VMP method for parameter estimation and the Kalman filter updates for the reference LSSM model are implemented using the software package **BayesPy**, introduced in [31].

2.3. Deep learning models

In the machine learning context, models are often associated with supervised learning tasks, where the model learns to make predictions based on input-output data. As a result, the observed data is represented as the set of inputs and outputs: $\{\mathbf{X}, \Delta\mathbf{y}\}$.

The inputs are defined as a tensor $\mathbf{X} \in \mathbb{R}^{N \times M \times L}$, where N is the number of observations, M is the number of input variables, and L is the number of preceding historical instances considered for all input variables given time t . The input variables are similar to (6), with a few additions and modifications which we cover in 3.1.

To promote physics related to the modeled system, the LSTM models are trained to model the change in indoor temperature $\Delta y^{(t)} = T_{\text{in}}^{(t+1)} - T_{\text{in}}^{(t)}$, unlike the physics-inspired reference model which models the indoor temperature directly. Our previous experience shows that modeling the differences results in more precise deep learning models for the physical system. Thus, the outputs $\Delta \mathbf{y} \in \mathbb{R}^N$ are the differences between the indoor temperature measurements of successive hours. As mentioned in 2.2, the time resolution of the observed data used in this work is hourly.

2.3.1. Long short-term memory networks

Recurrent Neural Networks (RNN) differ from standard feedforward networks in their ability to incorporate feedback loops, allowing them to utilize previous model states in their computations [32]. However, RNNs often face challenges such as vanishing or exploding gradients and a limited capacity to model seasonality [33]. To address these issues, Long Short-Term Memory (LSTMs) networks were developed, incorporating internal gating mechanisms that enable learning of long-term dependencies [34]. LSTMs are specifically designed to mitigate the vanishing gradient problem by dynamically learning pathways and employing so-called adaptive forgetting to reset model memory at appropriate time intervals [35].

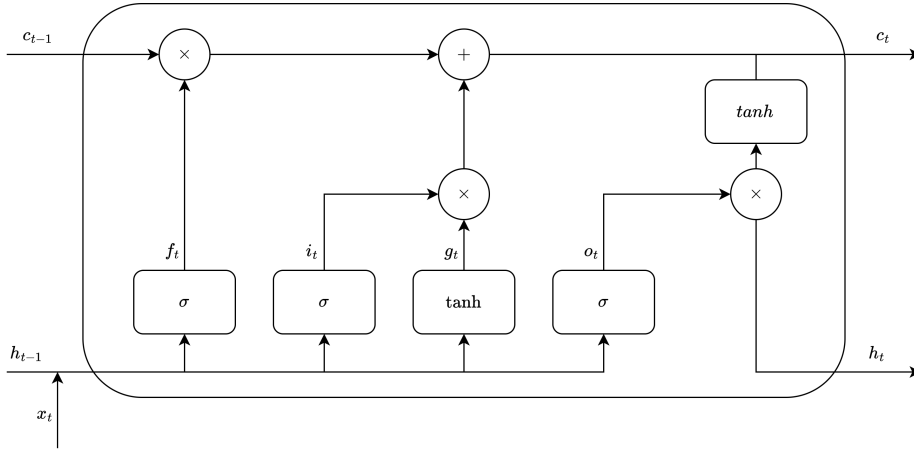


Figure 2: Structure of LSTM unit

The structure of an LSTM layer consists of hidden units (Figure 2) that are connected recurrently. The hidden unit consists of the forget gate $\mathbf{f}^{(t)}$, the input gate $\mathbf{i}^{(t)}$ and the output gate $\mathbf{o}^{(t)}$ are responsible for inserting new information into the system, determining which information should be discarded and which will be modified at the output. The following formulation of the architecture is given by [36]:

$$\begin{aligned}\mathbf{i}^{(t)} &= \sigma(\mathbf{W}_{xi}\mathbf{X}^{(t)} + \mathbf{W}_{hi}\mathbf{h}^{(t-1)} + \mathbf{b}_i), \\ \mathbf{f}^{(t)} &= \sigma(\mathbf{W}_{xf}\mathbf{X}^{(t)} + \mathbf{W}_{hf}\mathbf{h}^{(t-1)} + \mathbf{b}_f), \\ \mathbf{o}^{(t)} &= \sigma(\mathbf{W}_{xo}\mathbf{X}^{(t)} + \mathbf{W}_{ho}\mathbf{h}^{(t-1)} + \mathbf{b}_o),\end{aligned}\tag{11}$$

where σ is a sigmoid activation function, \mathbf{W}_{xi} , \mathbf{W}_{xf} , \mathbf{W}_{xo} , \mathbf{W}_{hi} , \mathbf{W}_{hf} , \mathbf{W}_{ho} are weight parameters from the input and the hidden states, \mathbf{X} is the input data to the cell, and \mathbf{b}_i , \mathbf{b}_f , \mathbf{b}_o are bias parameters. The learning process in LSTMs is mainly performed by the cell state $\mathbf{c}^{(t)}$, which is responsible for storing and managing the long-term memory of the model. The cell state is updated by performing element-wise multiplication of the gates and adding the result to the previous state, as modified by the forget gate. The input node $\mathbf{q}^{(t)}$ and the cell state are updated by:

$$\begin{aligned}\mathbf{q}^{(t)} &= \tanh(\mathbf{W}_{xg}\mathbf{X}^{(t)} + \mathbf{W}_{hg}\mathbf{h}^{(t-1)}), \\ \mathbf{c}^{(t)} &= \mathbf{f}^{(t)}\mathbf{c}^{(t-1)} + \mathbf{i}^{(t)}\mathbf{q}^{(t)},\end{aligned}\tag{12}$$

where \mathbf{W}_{xg} and \mathbf{W}_{hg} are weight parameters and \mathbf{b}_o is a bias parameter. The output gate $\mathbf{o}^{(t)}$ generates a selector vector based on both the previous hidden state and current inputs at time t , which functions similarly to the input gate. The hidden state is computed by combining the selector vector and the output candidate vector computed by

$$\mathbf{h}^{(t)} = \mathbf{o}^{(t)} \tanh(\mathbf{c}^{(t)}).\tag{13}$$

We construct a model from one LSTM unit, which takes the input \mathbf{X} with one layer, from which the final hidden state \mathbf{h} is given as input to the linear layer. The linear layer is then followed by a ReLU activation function and a second linear layer, used as an output layer.

Finally, we remark that the loss function used in the training is the mean absolute error (MAE):

$$\text{MAE} = \frac{1}{N-1} \sum_{j=1}^{N-1} |\Delta \mathbf{y}_i - \Delta \hat{\mathbf{y}}_i|, \quad (14)$$

where $\Delta \hat{\mathbf{y}}$ is the vector of predictions extracted from the final output layer.

2.3.2. Bayesian LSTM

A *Bayesian Neural Network* (BNN) is a machine learning approach that incorporates probabilistic modeling into a traditional feedforward neural network by treating the weights and biases as random variables, rather than fixed values. This allows for uncertainty quantification in predictions and enhances the model’s robustness to overfitting. The Bayesian aspect arises from assigning prior distributions to the weights and biases, and in this context, the training amounts to estimating the corresponding posterior distribution using Bayes’ theorem [37]. Despite the benefits of BNN, feedforward neural networks have proven to be disadvantaged against RNNs when forecasting time series [38]. This is typically due to the lack of information about past states.

Moreover, it is important to note that not all parameters in a BNN need to be treated as stochastic to achieve theoretical expressivity and gain the predictive performance of a fully stochastic neural network [39]. Since the optimized parameter space is smaller, partial stochastic neural networks can outperform fully stochastic neural networks in accuracy and training time. However, careful selection of the stochastic layer is crucial, as not all architectures may meet the criteria for effective probabilistic prediction.

Therefore, we propose a partially stochastic neural network containing an LSTM layer, a Bayesian linear layer, and a basic linear layer, forming an architecture we refer to as *Bayesian LSTM*. To illustrate this idea, let us lump the weights and biases into a parameter vector \mathbf{Z} , so we can write the posterior distribution as

$$p(\mathbf{Z} \mid \{\mathbf{X}, \Delta \mathbf{y}\}) \propto \exp \left(-\frac{1}{\ell} \|\Delta \mathbf{y} - \Psi(\mathbf{X}; \mathbf{Z})\|_1 \right) p(\mathbf{Z}); \quad (15)$$

where the prior $p(\mathbf{Z})$ is set as Gaussian $\mathcal{N}(\mathbf{0}, \beta^2 \mathbf{I})$, and the likelihood term corresponds to a multivariate Laplace distribution with fixed scale parameter $\ell = 1$, which is essentially the probabilistic version of the MAE loss in (14). Moreover, the operator $\Psi(\mathbf{X}; \mathbf{Z})$ in the likelihood term denotes the action of the Bayesian LSTM for a given \mathbf{X} and \mathbf{Z} , generating the predictive values $\Delta \hat{\mathbf{y}}$ as discussed in 2.3.1.

Due to the complexity of the posterior (15), we approximate it using the variational inference as described in 2.1. Hence, similar to the reference model in 2.2, the posterior in (15) is estimated by maximizing the ELBO (3). We assume our variational approximation to be Gaussian and factorize according to (4). The primary benefit of our Bayesian LSTM model is its ability to mitigate overfitting – a prevalent issue in deterministic neural networks – by performing probabilistic inference of the uncertain parameters.

3. Experiments

We describe the experimental settings for comparing the predictive performance between the three methods introduced in 2, and present the results.

3.1. Dataset

The dataset is collected by a private company specializing in MPC of central-heated residential buildings. The indoor temperature data are the averages of the sensor measurements at each apartment of the building. The space-heating circuit’s supply temperature data are measured at the heating substation. The outdoor temperature and solar irradiation data are from the weather data provider of the company.

The dataset contains hourly time series data for a total of $S = 100$ buildings from at least 3 years between 2017 and 2022. Since the heating season in Nordic countries focuses on months between September and May, the models are trained by excluding the data from the summer months. During the summer months, the heating systems are shut off, and therefore the indoor temperature cannot be affected by controlling the supply water temperature of the space-heating circuit.

Model fitting and training. As each building and heating system has different dynamics, all models are trained for the S buildings separately.

Everything related to the inputs and outputs of the reference model are covered in 2.2. The reference model parameter estimation is done using the data from the last 500 heating season days before September 2021.

For the LSTM models, all heating season data before September 2021 is split randomly into *training* and *validation* sets with a ratio of 9-to-1. As stated in 2.3, the LSTM models are trained to predict the change in indoor temperature between successive hours $T_{\text{in}}^{t+1} - T_{\text{in}}^t$. The input variables of the LSTM models (presented in Table 1) are feature engineered to inform the black-box models about the physics of the system: $T_{\text{sup}} - T_{\text{in}}$ and Φ_{rad} quantify the heat brought to the building by the heating system and solar irradiation, while $T_{\text{out}} - T_{\text{in}}$ describes the heat leaking through the envelope to the environment. The disturbance effect from internal heat sources is modeled by using a function ξ , which simply maps time t to an integer value based on the hour of the week: 1–24 for non-business-day and 25–48 for business-day hours. Additionally, we include the azimuth and elevation angles of the sun, α_{azi} and α_{ele} , calculated based on the GPS coordinates of the building using the software package `pvlb` [40, 41]. These two additional variables enhance the modeling of the solar effect based on seasonality and building orientation. Since the LSTM models are capable of modeling complex non-linear relationships such as thermal lag effects, the inputs do not just contain the latest realizations of the inputs, but a total of 6 latest values.

Variable	Description	Unit
$T_{\text{sup}} - T_{\text{in}}$	ΔT between supply water and inside air	$^{\circ}\text{C}$
$T_{\text{out}} - T_{\text{in}}$	ΔT between outside and inside air	$^{\circ}\text{C}$
Φ_{rad}	Global horizontal irradiation of the sun	W/m^2
α_{ele}	Elevation angle of the sun	$^{\circ}$
α_{azi}	Azimuth angle of the sun	$^{\circ}$
$\xi(t)$	An integer value based on the hour of the week	-

Table 1: Input variables of the LSTM models.

The reference model’s parameter estimation averaged under 5 seconds per building. In comparison, training times averaged 4 minutes for the standard LSTM and 8 minutes for the Bayesian variant.

Predictions. The *test* set contains data from October 2021 to April 2022. From the test dataset, we select $T = 100$ evenly distributed hourly timestamps t_i ($i = 1, \dots, T$), with 50 hour interval. Starting from these timestamps, we generate $S \cdot T = 10000$ indoor temperature prediction sequences into a prediction horizon of length $H = 48$ using all three models. Thus, all T_{in} predictions of a single model are denoted as a matrix $\hat{\mathbf{Y}} \in \mathbb{R}^{(S \cdot T) \times H}$. The ΔT_{in} predictions of the LSTM models are transformed into T_{in} predictions by cumulatively adding the predicted differences to the latest indoor temperature measurement the model had available given the starting point t_i . Because T_{in} is included in the LSTM model inputs, after the first prediction into H , the upcoming predictions into the prediction horizon are affected by the previous predictions. In the reference model, the same applies inherently due to the LSSM formulation.

The average computation time for a 48-hour indoor temperature prediction varied as follows across models: the reference model completed predictions in 0.008 seconds, compared to 0.17 seconds for the LSTM and 0.31 seconds for the Bayesian LSTM.

3.2. Results

In the MPC application for which the models are developed, prediction sequences of length $H = 48$ are updated every hour after observing new data. Therefore, for keeping the system state stable at the set point value and minimizing overheating with MPC, we are mostly interested in the models’ ability to create short-term predictions. However, the long-term predictions are important for optimal control planning based on the weather forecasts to achieve some of the additional optimization objectives, such as minimizing power peaks by pre-heating at appropriate times.

Prior selection for the Bayesian LSTM. The Bayesian LSTM is tested using three prior variances β^2 : 10^{-2} , 10^{-3} , and 10^{-4} . We generate $\hat{\mathbf{Y}} \in \mathbb{R}^{(S \cdot T) \times H}$ with Bayesian LSTMs trained using the three different prior variances. We then look at predictions into different horizon lengths $K \in [1, 6, 48]$ and calculate the

Root Mean Squared Errors (RMSE) w.r.t. measurements $\mathbf{Y} \in \mathbb{R}^{(S \cdot T) \times H}$ along the horizon lengths K as

$$\epsilon_i^{\text{hor}} = \sqrt{\frac{\sum_{j=1}^K (\mathbf{Y}_{i,j} - \hat{\mathbf{Y}}_{i,j})^2}{K}}, \quad i = 1, \dots, S \cdot T. \quad (16)$$

The respective RMSE distributions are shown in Figure 3.

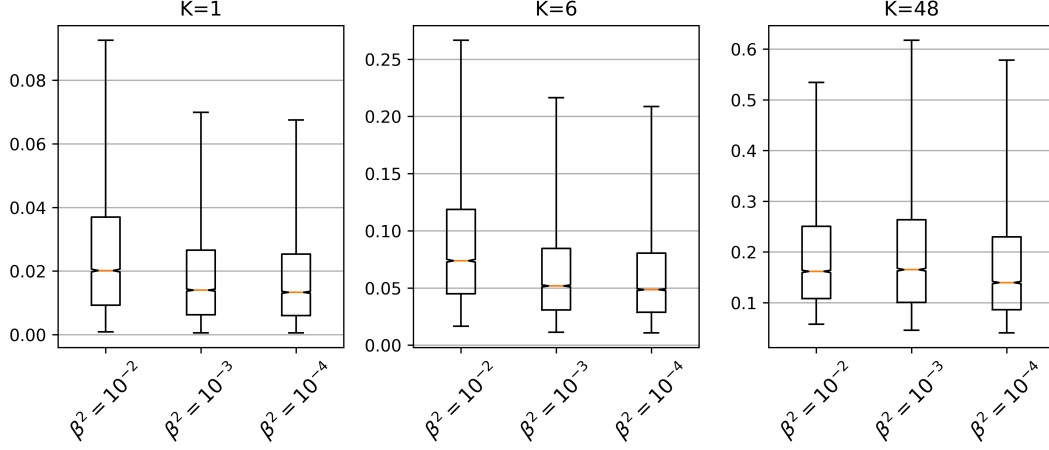


Figure 3: Bayesian LSTM performance with different prior variances β^2 as RMSE (16) for different prediction horizon lengths. Orange lines are the RMSE distribution medians, while boxes and whiskers indicate the 50% and 95% confidence intervals, respectively. Note the different scales on the Y-axis.

In addition to the predictive performance, it needs to be considered at which value the KL divergence (2) converges during the training process. Since KL divergence measures the dissimilarity between the true and the approximate distribution, the closer we get to zero, the better the posterior approximation.

For the Bayesian LSTMs with prior variances of 10^{-2} and 10^{-3} , KL divergence converged to values less than 1. Although the Bayesian LSTM with prior variance of 10^{-4} produces the best predictions, its KL divergence is 100 times larger than the others. A small variance in combination with a large KL divergence suggests too restrictive prior. This can lead to instability or overfitting, as the model may not effectively regularize its weights. Therefore, as the prior $\mathcal{N}(0, 10^{-3})$ achieves good predictive performance and low KL divergence for the posterior approximation, we select it for the Bayesian LSTM employed for the comparative experiments of the study.

Predictive performance. Figure 4 shows the 48-hour prediction sequences for two randomly selected test samples. Because the uncertainty of successive predictions are independent, the uncertainty of the Bayesian LSTM into the prediction horizon is calculated by accumulating the standard deviations of each prediction in the sequence.

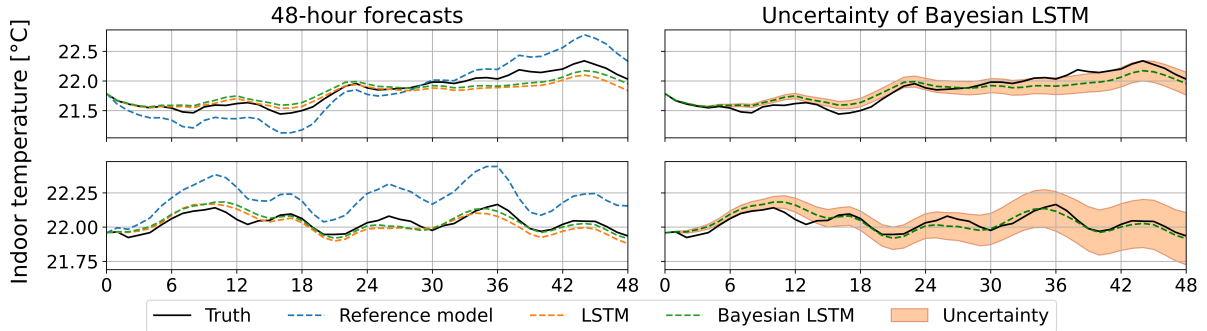


Figure 4: 48-hour predictions for two test samples with the different models. Bayesian LSTM prediction uncertainties are visualized separately on the right-hand side plots. Uncertainty is measured as the cumulative standard deviation of 10 predictions generated with the Bayesian LSTM.

To compare the predictive performance of the reference model, the LSTM, and the Bayesian LSTM, we use the same method with the RMSE metric (16) as we did when selecting the prior variance for the

Bayesian LSTM. The results are shown in Figure 5. Both LSTM models outperform the reference model across the different prediction horizon lengths, especially when it comes to longer prediction horizons. The short-term predictions are also significantly more accurate with a tighter RMSE distribution. The predictive performance between the LSTM and its Bayesian variant are more or less equal, although the Bayesian LSTM falls off ever so slightly for longer prediction horizons.

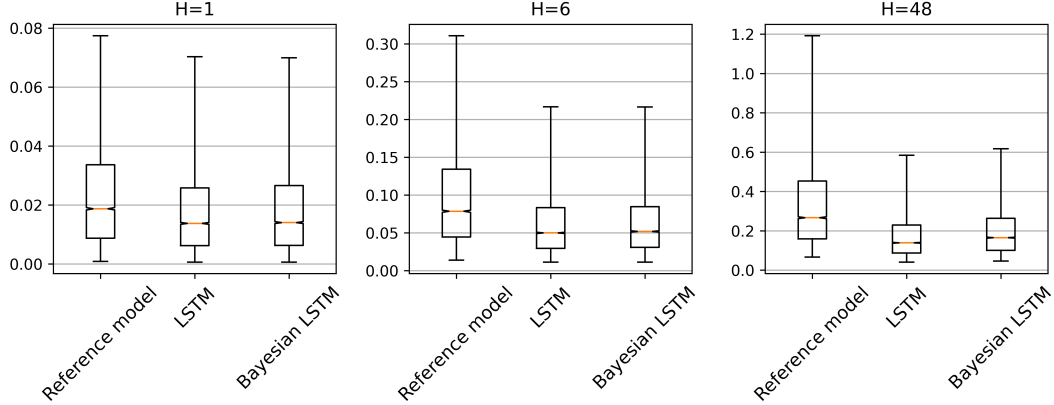


Figure 5: Performance of the three models as RMSE (16) for different prediction horizon lengths. Orange lines are the RMSE distribution medians, while boxes and whiskers indicate the 50% and 95% confidence intervals, respectively. Note the different scales on the Y-axis.

To evaluate how much the model predictions $\hat{\mathbf{Y}} \in \mathbb{R}^{(S \cdot T) \times H}$ drift from the measured truth $\mathbf{Y} \in \mathbb{R}^{(S \cdot T) \times H}$ when predicting into the prediction horizon of length $H = 48$, we calculate the average drift over our test samples w.r.t. prediction horizon length using a similar metric to (16), but this time averaging along the test samples:

$$\epsilon_j^{\text{dri}} = \sqrt{\frac{\sum_{i=1}^{(S \cdot T)} (\mathbf{Y}_{i,j} - \hat{\mathbf{Y}}_{i,j})^2}{S \cdot T}}, \quad j = 1, \dots, H. \quad (17)$$

The average prediction drifts for all three models are visualized in Figure 6. The results show that LSTM models achieve progressively better performance relative to the reference model as the prediction horizon lengthens.

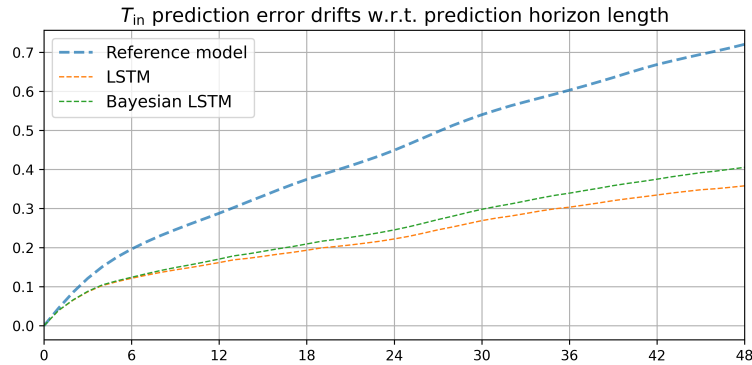


Figure 6: Average prediction drifts (17) of the models. Both LSTM methods perform significantly better compared to the reference model.

As discussed earlier, we are more interested about the short-term over the long-term predictive accuracy. Hence, to compare the performance of the models using a single metric aligned with what we are interested in, the prediction drift series visualized in Figure 6 is averaged using linear- and sigmoid-shaped weight functions. These functions give decreasing weights for the RMSE values w.r.t. prediction horizon length. The sigmoid function gives more weight to the short-term prediction accuracy compared to the linear function. The performance scores calculated this way are shown in Table 2 for all three models.

	Unweighted	Sigmoid	Linear
Grey-box	0.436	0.145	0.161
LSTM	0.225	0.079	0.086
Bayesian LSTM	0.247	0.084	0.093

Table 2: Predictive performance scores for the three models calculated by averaging the prediction accuracy drifts w.r.t. prediction horizon length (see Figure 6) using different weight functions.

4. Conclusions

We developed a Bayesian LSTM to model indoor temperatures in 100 centrally heated residential buildings and compared its 48-hour predictive performance against an industrial reference LSSM and a deterministic LSTM. The LSTMs outperformed the reference model significantly in both short- and long-term predictions, roughly halving the prediction errors, on average. While the two LSTM variants showed similar accuracy, the Bayesian version offers better interpretability and generalization due to its probabilistic nature. Integrating these models into real-world heating MPC has a huge potential to improve control accuracy, enhancing energy efficiency and thermal comfort.

The LSTMs’ superior performance stems from their ability to capture complex nonlinear thermodynamics, including: thermal lag effects (heat storage in building structures), solar gain variations (accounting for sun angles), and multi-step dependencies in input variables.

For industrial MPC deployment, computational efficiency of the LSTMs could be improved to enable (1) faster hourly predictions in real-time control optimization, and (2) lower computational costs of frequent model updates to reflect changes in system dynamics. Hence, we leave as future work the following:

- (i) Architecture optimization (e.g., dimension reduction via sensitivity analysis or principal component analysis).
- (ii) Hyperparameter tuning (batch size, learning rates, initialization).
- (iii) Building heating dynamics exhibit seasonal patterns, slow trends, and sudden shifts (e.g., from physical modifications). Future work could also focus on adaptive methods that balance learning from new data and discarding outdated information, possibly via time-evolving parameters [42].
- (iv) While our LSTMs incorporate physics-based feature engineering, further integration of domain knowledge could enhance generalization, especially with limited or noisy training data.

5. Acknowledgments

We would like to give special thanks to Jaakko Luttinen for his work on the reference method, and Alexander Ilin for his involvement in conceptualization of the project. Furthermore, we thank Danfoss Leanheat for providing the data used in the study. This work was supported by the Finnish Ministry of Education and Culture’s Pilot for Doctoral Programmes (Pilot project Mathematics of Sensing, Imaging and Modelling) and Research Council of Finland (Flagship of Advanced Mathematics for Sensing and Imaging and Modeling grant 359183, Centre of Excellence of Inverse Modelling and Imaging grant 353095). The research of Jana de Wiljes has been partially funded by the Deutsche Forschungsgemeinschaft (DFG)-Project-ID 318763901 - SFB1294. Furthermore, this project has received funding from the European Union under the Horizon Europe Research & Innovation Programme (Grant Agreement no. No 101188131 UrbanAIR). Views and opinions expressed are however those of author(s) only and do not necessarily reflect those of the European Union. Neither the European Union nor the granting authority can be held responsible for them.

References

- [1] International Energy Agency (IEA), [World Energy Outlook 2024](#), 2024.
- [2] United Nations Environment Programme, [Global Status Report for Buildings and Construction](#), 2024.
- [3] M. González-Torres, L. Pérez-Lombard, J. F. Coronel, I. R. Maestre, D. Yan, A review on buildings energy information: Trends, end-uses, fuels and drivers, *Energy Reports* 8 (2022) 626–637.
- [4] D. Ürge Vorsatz, L. F. Cabeza, S. Serrano, C. Barreneche, K. Petrichenko, Heating and cooling energy trends and drivers in buildings, *Renewable and Sustainable Energy Reviews* 41 (2015) 85–98.

- [5] R. Fazeli, B. Davidsdottir, J. H. Hallgrímsson, Residential energy demand for space heating in the Nordic countries: Accounting for interfuel substitution, *Renewable and Sustainable Energy Reviews* 57 (2016) 1210–1226.
- [6] Y. Yao, D. K. Shekhar, State of the art review on model predictive control (MPC) in heating ventilation and air-conditioning (HVAC) field, *Building and Environment* 200 (2021) 107952.
- [7] S. Taheri, P. Hosseini, A. Razban, Model predictive control of heating, ventilation, and air conditioning (HVAC) systems: A state-of-the-art review, *Journal of Building Engineering* 60 (2022) 105067.
- [8] J. Drgoňa, J. Arroyo, I. Cupeiro Figueroa, D. Blum, K. Arendt, D. Kim, E. P. Ollé, J. Oravec, M. Wetter, D. L. Vrabie, L. Helsen, All you need to know about model predictive control for buildings, *Annual Reviews in Control* 50 (2020) 190–232.
- [9] L. Ramadan, I. Shahrour, H. Mroueh, F. H. Chehade, Use of machine learning methods for indoor temperature forecasting, *Future internet* 13 (2021) 242.
- [10] C. Xu, H. Chen, J. Wang, Y. Guo, Y. Yuan, Improving prediction performance for indoor temperature in public buildings based on a novel deep learning method, *Building and environment* 148 (2019) 128–135.
- [11] F. Mtibaa, K.-K. Nguyen, M. Azam, A. Papachristou, J.-S. Venne, M. Cheriet, LSTM-based indoor air temperature prediction framework for HVAC systems in smart buildings, *Neural Computing and Applications* 32 (2020) 17569–17585.
- [12] L. Ma, Y. Huang, J. Zhang, T. Zhao, A model predictive control for heat supply at building thermal inlet based on data-driven model, *Buildings (Basel)* 12 (2022) 1879.
- [13] F. Elmaz, R. Eyckerman, W. Casteels, S. Latré, P. Hellinckx, CNN-LSTM architecture for predictive indoor temperature modeling, *Building and environment* 206 (2021) 108327.
- [14] B. Jiang, H. Gong, H. Qin, M. Zhu, Attention-LSTM architecture combined with Bayesian hyperparameter optimization for indoor temperature prediction, *Building and environment* 224 (2022) 109536.
- [15] Z. Fang, N. Crimier, L. Scanu, A. Midelet, A. Alyafi, B. Delinchant, Multi-zone indoor temperature prediction with LSTM-based sequence to sequence model, *Energy and buildings* 245 (2021) 111053.
- [16] F. Bünnig, B. Huber, A. Schalbetter, A. Aboudonia, M. Hudoba de Badyn, P. Heer, R. S. Smith, J. Lygeros, Physics-informed linear regression is competitive with two machine learning methods in residential building MPC, *Applied Energy* 310 (2022) 118491.
- [17] D. T. Mirikitani, N. Nikolaev, Recursive bayesian recurrent neural networks for time-series modeling, *IEEE Transactions on Neural Networks* 21 (2010) 262–274.
- [18] R. Wen, K. Torkkola, B. Narayanaswamy, D. Madeka, A multi-horizon quantile recurrent forecaster, *arXiv preprint arXiv:1711.11053* (2017).
- [19] A. M. Alaa, M. van der Schaar, Frequentist uncertainty in recurrent neural networks via blockwise influence functions, in: H. Daumé III, A. Singh (Eds.), *Proceedings of the 37th International Conference on Machine Learning*, volume 119, PMLR, 2020, pp. 175–190.
- [20] C. Xu, Y. Xie, Conformal prediction interval for dynamic time-series, in: M. Meila, T. Zhang (Eds.), *Proceedings of the 38th International Conference on Machine Learning*, volume 139, PMLR, 2021, pp. 11559–11569.
- [21] K. Stankevičiūtė, A. M. Alaa, M. van der Schaar, Conformal time-series forecasting, in: *Advances in Neural Information Processing Systems*, volume 34, 2021, pp. 14485–14497.
- [22] A. Gelman, J. Carlin, H. Stern, D. Dunson, A. Vehtari, D. Rubin, *Bayesian Data Analysis*, Third Edition, Chapman & Hall/CRC Texts in Statistical Science, Taylor & Francis, 2013.
- [23] M. I. Jordan, Z. Ghahramani, T. S. Jaakkola, L. K. Saul, *An Introduction to Variational Methods for Graphical Models*, Springer Netherlands, Dordrecht, 1998, pp. 105–161. doi:[10.1007/978-94-011-5014-9](https://doi.org/10.1007/978-94-011-5014-9).
- [24] C. Bishop, *Pattern recognition and machine learning*, Information science and statistics, Springer, 2006.
- [25] J. Winn, C. M. Bishop, Variational message passing, *Journal of Machine Learning Research* 6 (2005) 661–694.
- [26] J. Luttinen, Fast variational Bayesian linear state-space model, in: *Machine Learning and Knowledge Discovery in Databases*, Springer, 2013, pp. 305–320.
- [27] A. Ionesi, On modeling and estimation techniques towards on-line applications in building energy management systems, 2019.
- [28] R. H. Shumway, D. S. Stoffer, *Time series analysis and its applications*, Springer, 2000.
- [29] D. E. Kirk, *Optimal control theory - An introduction*, 1 Edition., Dover Publications, 1998.
- [30] S. Särkkä, L. Svensson, *Bayesian Filtering and Smoothing*, 2 Edition., Cambridge University Press, 2023.
- [31] J. Luttinen, Bayespy: Variational bayesian inference in python, *Journal of Machine Learning Research* 17 (2016) 1–6.
- [32] I. Goodfellow, Y. Bengio, A. Courville, *Deep learning*, MIT Press, 2016.
- [33] H. Hewamalage, C. Bergmeir, K. Bandara, Recurrent neural networks for time series forecasting: Current status and future directions, *International journal of forecasting* 37 (2021) 388–427.
- [34] S. Hochreiter, J. Schmidhuber, Long short-term memory, *Neural computation* 9 (1997) 1735–1780.
- [35] F. A. Gers, J. Schmidhuber, F. Cummins, Learning to forget: Continual prediction with LSTM, *Neural Computation* 12 (2000) 2451–2471.
- [36] D. Mora-Mariano, A. Flores-Tlacuahuac, Bayesian LSTM framework for the surrogate modeling of process engineering systems, *Computers & Chemical Engineering* 181 (2024) 108553.
- [37] R. M. Neal, *Bayesian learning for neural networks*, volume 118, Springer Science & Business Media, 2012.
- [38] D. Brezak, T. Bacek, D. Majetic, J. Kasac, B. Novakovic, A comparison of feed-forward and recurrent neural networks in time series forecasting, in: 2012 IEEE Conference on Computational Intelligence for Financial Engineering & Economics (CIFER), IEEE, 2012, pp. 1–6. doi:[10.1109/CIFER.2012.6327793](https://doi.org/10.1109/CIFER.2012.6327793).
- [39] M. Sharma, S. Farquhar, E. Nalisnick, T. Rainforth, Do bayesian neural networks need to be fully stochastic?, in: *Proceedings of The 26th International Conference on Artificial Intelligence and Statistics*, volume 206 of *Proceedings of Machine Learning Research*, PMLR, 2023, pp. 7694–7722.
- [40] W. F. Holmgren, C. W. Hansen, M. A. Mikofski, pvlib python: a python package for modeling solar energy systems, *Journal of Open Source Software* 3 (2018) 884.
- [41] K. S. Anderson, C. W. Hansen, W. F. Holmgren, A. R. Jensen, M. A. Mikofski, A. Driesse, pvlib python: 2023 project update, *Journal of Open Source Software* 8 (2023) 5994.
- [42] L. Rimella, N. Whiteley, Hidden markov neural networks, *Entropy* 27 (2025).